Shear-Mediated Crystallization of Isotactic Polypropylene: The Role of Long Chain−Long Chain Overlap

Motohiro Seki,[†] Derek W. Thurman,[‡] James P. Oberhauser,[‡,§] and Julia A. Kornfield*[,‡]

Yokkaichi Research Center, Mitsubishi Chemical Corporation, No 1, Toho, Yokkaichi, Mie 510-0848 Japan; and 210-41, Division of Chemistry and Chemical Engineering, California Institute of Technology, Pasadena, California 91125

Received July 30, 2001

ABSTRACT: The role of long chains in shear-mediated crystallization was studied by in situ rheo-optical measurements and ex situ microscopic observations. To elucidate the effects of long chains, we prepared model blends in which fractionated isotactic polypropylene (iPP) (denoted L-PP) with high molecular weight (MW) and narrow molecular weight distribution was blended with a metallocene iPP (Base-PP) with lower molecular weight. The concentration of L-PP (c) was varied ranging from 0 to twice the concentration (c^*) at which L-PP coils overlap. The crystallization of all blends after cessation of transient shearing was accelerated, while the quiescent crystallization kinetics were not affected by the addition of L-PP. A distinctive change in the development of birefringence after shearing was observed when the wall shear stress (σ_w) exceeded a critical value (σ^*). Below σ^*, irrespective of c, the birefringence after transient shearing increased gradually, reaching a small value at the end of crystallization. Above σ^*, a brief interval of shear induced highly oriented growth, manifested in the birefringence after cessation of flow and growing stronger and reaching a large value as crystallization proceeded. Further, the rate of growth of the birefringence exhibited a strong, nonlinear c dependence. The morphology of the skin layer showed a shish kebab type structure observed by TEM for samples subjected to stresses above σ^*. The number density and thickness of shish were affected by c and changed drastically at c near the overlap concentration of the long chains. This indicates that the role of long chains in shear-induced oriented crystallization is cooperative (rather than a single chain effect), enhanced by long chain−long chain overlap.

1. Introduction

Key polymer processing technologies (e.g., injection molding) impose intense shearing flows and have prompted investigation into the crystallization of polymer melts induced by shearing. Empirically, it is known that processing conditions profoundly alter the rate of solidification, the semicrystalline morphology, and, ultimately, material properties.[1−7] The strong effects of flow are attributed to the perturbation of chain configuration by flow. Keller and co-workers[8,9] have studied flow-induced crystallization in polymer solutions, where interactions between molecules can be minimized, to describe the underlying mechanisms of polymer crystallization from the oriented state, partly based on the detailed study of "shish kebab" structures grown from stirred solutions.[10] It has been generally believed that extension of macromolecules promotes the formation of long threadlike structures oriented in the stress direction, and these filaments serve as nucleating surfaces for radial growth of chain-folded lamellae under elongational flow.[11] This "row nucleated structure" model has found great utility in describing the morphology resulting from elongational flow-induced crystallization of bulk polymers, where the connectivity of a chain and entanglements between chains restrict the segmental motion of the molecules.[12] Similarly, this model has been used to describe the formation of shish kebab morphology caused by shear flow where full extension of individual chains is unlikely, but extension of portions of the chain can occur between topological constraints imposed by surrounding molecules in the melt.[13]

It has also been inferred that the flow-induced changes in crystallization kinetics and the induction of the shish kebab structure are strongly affected by long chains.[14−19] The evidence is based on samples that have broad distributions of molecular weight and molecular regularity. This has presented a major obstacle to (1) defining what is meant by the long chains, (2) proving that their role is due specifically to length and not to a more perfect molecular structure, and (3) discerning how their impact varies with concentration to gain deeper insight into the physics of their effect. Further, when comparing materials of different average length, a number of investigators have used experiments performed at a given deformation rate.[7,14−15,17−18,20−21] This choice makes it difficult to attribute the differences to molecular length per se, since the comparisons are made at very different stresses. Since the effects of stress are known to be very strong, including qualitative changes in kinetics and morphology upon crossing threshold stress levels, comparisons made at fixed stress are needed to probe the effects of chain length and its distribution.

To overcome the limitations of poorly defined materials, we follow the approach of Kumaraswamy et al.,[22] who recently demonstrated that preparation of binary blends of narrow distribution isotactic polypropylenes (iPPs) provides a route to model materials in which the length and concentration of long chains are known and can be systematically varied. To expose the effect of long chains on the response during and after shear, we adopt the "short-term shearing" approach of Janeschitz-

* To whom correspondence should be addressed.
[†] Mitsubishi Chemical Corporation.
[‡] California Institute of Technology.
[§] Present address: Department of Chemical Engineering, University of Virginia, Charlottesville, VA 22904-4741.

10.1021/ma011359q CCC: $22.00
Published on Web 02/28/2002

Table 1. Characteristics of Base and Fractionated i-PP

sample	M_w[a] (kg/mol)	M_n[a] (kg/mol)	M_w/M_n	[mmmm][b] (mol %)	T_m[c] (°C)
base-PP	186.0	80.9	2.3	96.0	148.3
L-PP	923.2	707.3	1.3	98.0	164.6

[a] Determined by GPC-MALLS. [b] ^{13}C NMR. [c] Apparent melting temperature obtained from peak position of DSC.

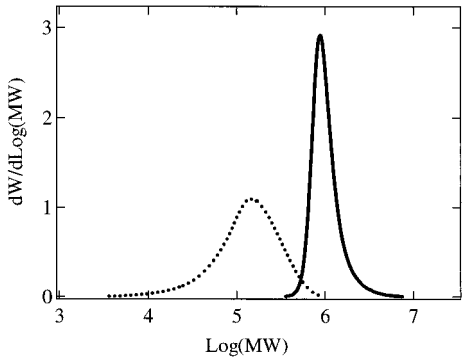

Figure 1. Molecular weight distribution for base-PP (dotted line) and L-PP (solid line) measured by GPC-MALLS.

Kriegl[23−26] and make comparisons of the effects of flow at a given shear stress. This approach allows us to overcome difficulties in interpretation of prior studies[16−18,20−21] that were complicated by one or more of the following: nonisothermal conditions, continuous flow during the entire crystallization process, and/or inability to access stresses that induce the transition to oriented growth. To evaluate structural changes during and after cessation of shearing, we use in situ rheo-optical measurements; to reveal final morphological changes, ex situ microscopic observations were performed.

2. Experimental Section

2.1. Materials. An iPP with moderate molecular weight (186 kg/mol) and narrow polydispersity in terms of both molecular weight ($M_w/M_n = 2.3$) and stereoregularity ([mmmm] = 96%) was provided by Dr. Robert Sammler (Dow Chemical Corp.) for use as a base polymer resin (base-PP). An iPP with much higher molecular weight (923 kg/mol), narrow PDI (M_w/M_n=1.3) and high stereoregularity ([mmmm] = 98%) (L-PP) was prepared by fractionation from a parent iPP polymerized with a Ziegler−Natta catalyst. Fractionation in terms of MW was performed by the solvent gradient method, in which the solvent composition of *o*-dichlorobenzene and diethylene glycol monomethyl ether in polymer solution was changed gradually.[27] The molecular characteristics of these two polypropylenes are summarized in Table 1, and the methods by which molecular characterization was performed are presented elsewhere.[28] The molecular weight distributions of Base-PP and L-PP are presented in Figure 1. The difference in stereoregularity led to a 5 °C difference in the apparent melting point of the two samples.

We prepared bidisperse blends with different concentrations of L-PP (c), varying c from 0 to twice the concentration (c^*) at which molecular coils of L-PP overlap each other. The overlap concentration, c^*, is[29,30]

$$c^* = \frac{3M_w}{4\pi(R_g^2)^{3/2} N_a} \quad (1)$$

where N_a is Avogadro's number. The characteristic ratio of weight-averaged radius of gyration to M_w of iPP ($\langle R_g^2\rangle/M_w^{0.5}$) is 0.39 according to SANS measurements,[31] leading to an estimated c^* of 7.0×10^{-3} g/cm^3 for L-PP. Blends are coded using the value of c/c^*. For example, B025 denotes the blend with $c/c^* = 0.25$. The blend compositions are summarized in Table 2.

Table 2. Blend Composition and Thermal Properties

blend	c[a] (g/cm^3)	c/c^*[a]	T_c[b] (°C)	ΔH_f[b] (J/g)	T_m[c] (°C)
B0	0	0	113.1	84.3	143.8
B025	1.76×10^{-3}	0.25	112.2	86.7	143.8
B05	3.51×10^{-3}	0.5	112.7	83.5	143.7
B1	7.00×10^{-3}	1.0	111.9	84.5	143.6
B2	1.39×10^{-2}	2.0	112.9	86.2	143.8

[a] Concentration of L-PP (c) and the critical concentration of L-PP obtained from eq 1 in the main text. [b] Crystallization temperature (T_c) and heat of fusion (ΔH_f) determined by the exothermal peak position and calorific value of DSC with the constant cooling condition of 5 °C/min from the melt (220 °C). [c] Apparent melting temperature (T_m) was determined by the peak temperature of DSC with heating rate of 5 °C/min.

Nogales et al. report preparing blends via melt extrusion blending.[32] To obtain a homogeneous mixture, we employed a solution blending method that avoids potential problems of degradation of the long chains or incomplete mixing due to the very different melt viscosities of L-PP and Base-PP. Base-PP and L-PP were weighed and codissolved in a 2.3% xylene solution at 140 °C for 20 min under nitrogen atmosphere and in the presence of an antioxidant (2000 ppm of IRGANOX1010, distributed by Ciba). A precipitate was obtained by pouring a fine stream of the hot xylene solution into a large excess (8:1) stirred of methanol, which was then filtered and dried under vacuum for 3 days at 80 °C. After further addition of 2000 ppm of a 1:1 mixture of two antioxidants, IRGAFOS168 and IRGANOX1010, the dried precipitate was press molded at 180 °C under 10 000 psi into an ingot sized to fit the sample reservoir for the shear experiment.

2.2. Rheo-Optical Measurements during Shear-Mediated Crystallization. The instrument for shear-mediated crystallization used in this study[33] can apply a well-defined thermal history and impose high wall shear stresses for a controlled duration. The flow cell was initially held at 215 °C and filled with polymer melt from the reservoir. The polymer in the flow cell was then held at 215 °C for 10 min[34] to erase any memory effects caused by the filling process. Finally, the sample was cooled to the crystallization temperature (T_c). When T_c was reached, a desired pressure drop was applied to drive shear flow through the channel for a brief shearing time t_s. All experiments described here were conducted at the same T_c of 137 °C. Temperature stability was maintained within ± 0.3 °C. Short-term shear pulses, corresponding to wall shear stresses (σ_w) of 0.07, 0.105, 0.13 and 0.14 MPa were applied for brief periods such that t_s was much less than the crystallization time at this temperature. The geometry of the flow cell (length/depth ∼ 100) limits the total experimental shear strain at the wall (γ_w), as described in the Supplementary Information of ref 22. The flow cell has a rectangular cross section with dimensions 63.5 mm × 6.35 mm × 0.5 mm (length × width × depth). The maximum t_s was determined to be that at which ca. 100 mg of supercooled polymer was extruded. To change total strain, the amount of polymer extruded (w_{ex}) was varied from about 30 to 100 mg.

The turbidity and birefringence were tracked to monitor the progress and anisotropy of crystallization. The optical train used for the measurements was the same as described previously.[35] The intensity of He−Ne laser light passing through crossed and parallel polarizers ($I_\perp$ and $I_\parallel$) was measured with photodiode detectors.[35] When depolarization is negligible, the birefringence (Δn), which is a measure of the mean anisotropy of the sample, is given by

$$\Delta n = \frac{\lambda}{\pi d}\sin^{-1}\left(\sqrt{\frac{I_\perp}{I_\parallel + I_\perp}}\right) \quad (2)$$

where λ is the wavelength of light (632.8 nm) and d is the thickness of the sample. Transmittance is defined as total

transmitted intensity ($I_{tot} = I_{\perp} + I_{||}$) normalized by a constant value of $I_{tot,0}$ before shearing.

2.3. Transmission Electron Microscopy (TEM). Sheared samples examined in the rheo-optical experiments were allowed to solidify at $T_c = 137$ °C in situ until the transmittance dropped to zero, after which the flow cartridge was removed and plunged into ice water. After the cartridge had cooled, the sample was removed and prepared for ex situ morphology studies. Ultrathin sections approximately 100 nm in thickness were cut at a position corresponding to the center of the optical window. A block face was cut, the sample was stained with ruthenium tetroxide for 2 h at 50 °C,[36] and then sections were cut from the block face using a microtome. Thin sections for both "through" and "edge" views were prepared (images in the flow-vorticity and flow-gradient planes, respectively). TEM observation was carried out using a JEOL TEM model JEM 1230 at 100 kV.

2.4. Optical Microscopy (OM). Thick sections (thickness = 10 μm) were taken in the flow-vorticity and flow-gradient planes and were subject to investigation under a polarization microscope.

2.5. DSC Measurements. In a differential scanning calorimeter (Perkin-Elmer DSC-7), the crystallization and the melting of iPPs were characterized at a scanning rate of 5 °C/min in N_2 atmosphere.

2.6 Measurement of Molecular Weight. Weight averaged molecular weight (M_w) and polydispersity of molar mass for iPPs were measured by GPC with on-line multiangle laser light scattering photometer (GPC-MALLS). The measurements were performed on a Waters model 150C with three polystyrene columns (SHODEX KF-806M from Showa Denko Co. Ltd.) at 413.2 K using a flow rate of 1.0 mL/min. The sample was injected as a 0.3 mL aliquot of a 1,2,4-trichlorobenzene solution with 2 mg/mL concentration. The differential refractometer was used to detect solute concentrations and specific refractive index increments. The MALLS model DAWN DSP from Wyatt Technology Corp., equipped with a He−Ne laser ($\lambda = 632.8$ nm), was connected with the GPC instrument. The ASTRA software package from Wyatt Technology Corp. was used for analyzing GPC data and scattering data, which were collected simultaneously at 17 scattering angles ranging from 18 to 155°. (Details are given in ref 28).

3. Results

3.1. Quiescent Crystallization Kinetics. The peak temperature and enthalpy change (ΔH_f) in the crystallization process were measured by differential scanning calorimetry (DSC) at a constant cooling rate. These values were almost identical for all blends and were ca. 112 °C and 85 J/g, respectively. Addition of L-PP to base-PP did not affect the crystallization kinetics under quiescent conditions, even though pure L-PP possesses fairly high crystallizability compared with base-PP due to its higher stereoregularity. Similarly, the turbidity half time, which is defined by the time at which the transmittance reaches one half, was approximately 6500 s at 137 °C for all blends (Figure 2) and virtually independent of *c*. Slight differences in the turbidity half time can be ascribed to variability in the temperature control.

3.2. Shear Mediated Crystallization. 3.2.1. Turbidity. Manifested by development of turbidity at earlier times, crystallization kinetics appear to accelerate with increasing σ_w even when t_s is reduced to hold the total applied strain nearly constant (Figure 3). The turbidity half time of the blends sheared at 0.14 MPa for the maximum t_s was approximately 10 times shorter than that for quiescent conditions. The addition of low concentrations of long chains (<2 wt %) only slightly alters the melt rheology. Therefore, these comparisons are made not only at fixed stress (hence nearly the same average level of segmental orientation due to flow) but also for similar shearing time and total applied strain.

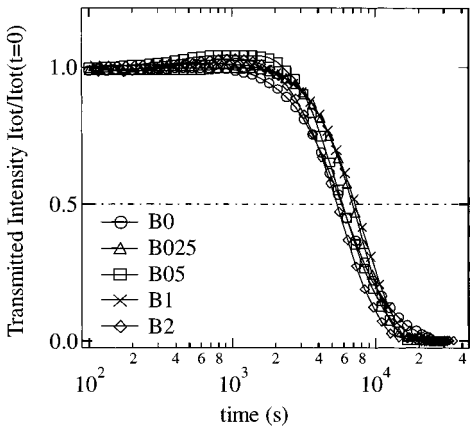

Figure 2. Turbidity of blends crystallized quiescently at 137 °C. ○, △, □, ×, and ◇ represent B0, B025, B05, B1, and B2, respectively.

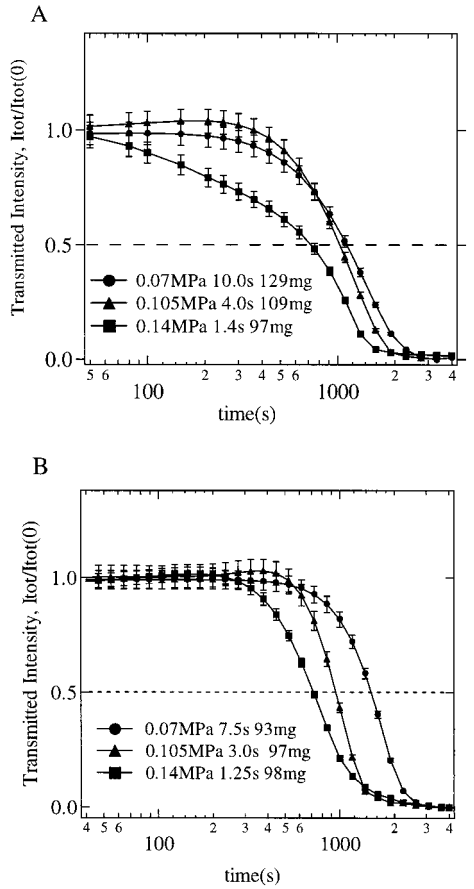

Figure 3. Turbidity of (A) B0 and (B) B1 during crystallization after short-term shearing ($t = 0$ defines beginning of shear) at $T_c = 137$ °C and various wall shear stresses for maximum shearing time (extruded mass was about 100 mg). ●, ▲, and ■ correspond to σ_w of 0.07, 0.105, and 0.14 MPa, respectively.

The turbidity half time also decreases with increasing t_s, but the dependence on t_s is much weaker than the dependence on σ_w (Figure 4).

3.2.2. Birefringence. Distinctive changes in the transient birefringence with applied stress indicate a critical stress level is necessary to induce highly oriented crystalline growth in the sample. Therefore, we define a "critical shear stress" (σ^*) necessary for this event.

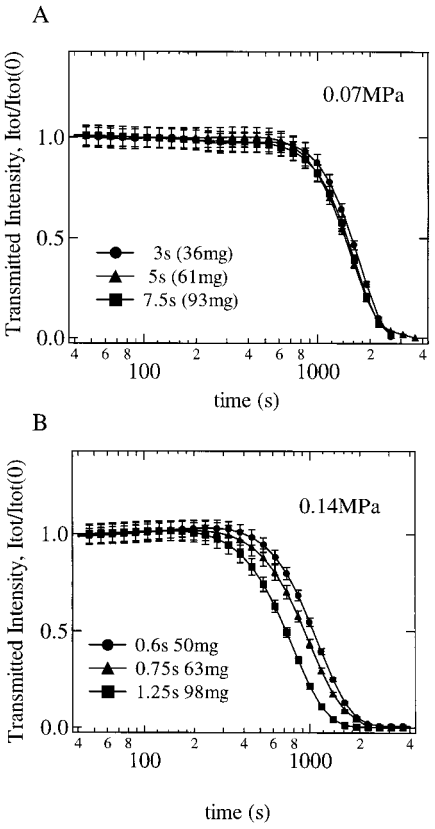

Figure 4. Turbidity of B1 during crystallization after short term shearing at $T_c = 137$ °C for σ_w of (A) 0.07 and (B) 0.14 MPa for various shearing times.

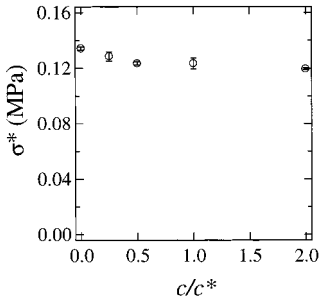

Figure 5. Critical shear stress (σ^*) needed to induce the transition to oriented growth plotted against long chain concentration (c/c^*). The value for σ^* was determined by measuring the depth of the highly birefringent skin in polarized light micrographs. The error bars indicate variation in the skin thickness rather than measuring error.

For the present samples, as described below, the critical shear stress was approximately $\sigma^* = 0.12$ MPa for all samples (Figure 5).

Below this threshold stress ($\sigma_w < \sigma^*$), the birefringence profiles show no evidence of highly oriented growth (Figure 6). The plots of $I_\perp/I_{tot}$ for B1 are representative of all blends during and after shearing at σ_w ranging from 0.07 to 0.13 MPa for different t_s (0.5 s $\leq t_s \leq$ maximum t_s). $I_\perp/I_{tot}$ during shearing exhibits a boxlike locus, which increases almost instantaneously to the plateau value and then drops to the baseline value, a response that is consistent with the applied pressure profile. $I_\perp/I_{tot}$ then increases gradually after cessation of flow, reaching a value around 0.1 at the end of the optical experiment (stopped when the transmittance falls to zero) regardless of c and σ_w ($\leq$0.13 MPa). The final value of $I_\perp/I_{tot}$ is the same as that for the quiescent experiment and can be attributed to multiple

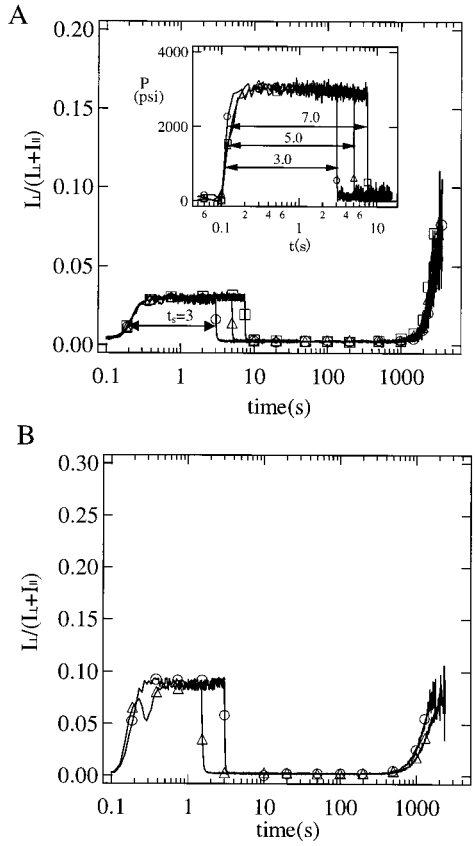

Figure 6. Relative intensity through crossed polarizers ($I_\perp/I_{tot}$) of B1 during short-term shearing at 137 °C and during the crystallization after cessation of shear. The inception of shear is taken to be $t = 0.1$ s since the first relevant decade is 0.1−1 s. (A) Shear pulse with $\sigma_w = 0.07$ MPa was applied for (○) 3.0, (△) 5.0, and (□) 7.5 s, with corresponding w_{ex} (mass extruded ∼ total strain) of 36, 61, and 93 mg, respectively. (B) Shear pulse at $\sigma_w = 0.105$ MPa was applied for (○) 3.0 and (△) 1.5 s; corresponding w_{ex} was 47 and 97 mg, respectively. A "boxlike" pressure profile was imposed during t_s (inset in A).

scattering leading to depolarization. However, shearing at $\sigma_w < 0.13$ MPa does induce some anisotropy in the sample. The delay time (t_d) between the cessation of shearing and the subsequent growth of $I_\perp/I_{tot}$ decreases with increasing σ_w and increasing c. Experiments performed on the blends at 0.0105 MPa for maximum t_s showed t_d of approximately 900 ± 100, 650 ± 50, 600 ± 50, 450 ± 30, 500 ± 30 s for B0, B025, B05, B1, and B2, respectively. The low turbidity at t_d ($I_{tot}/I_{tot,0} \approx 1.0$) suggests that this rise in $I_\perp/I_{tot}$ is not due to depolarization. The effect of t_s on t_d is very weak but hints at a trend of decreasing t_d with increasing t_s.

For $\sigma_w \geq \sigma^*$, the birefringence profiles show evidence of highly anisotropic crystallization (Figure 7). The values of $I_\perp/I_{tot}$ during crystallization after shearing attain remarkably large values compared with results at lower σ_w ($\sigma_w \leq 0.13$ MPa). For B025 with $\sigma_w = 0.14$ MPa and $t_s = 0.5$ s (less than the maximum t_s), $I_\perp/I_{tot}$ reaches 0.4, more than four times larger than the ultimate value following shear at a slightly lower σ_w and maximum t_s. The development of $I_\perp/I_{tot}$ for shear at 0.14 MPa is strongly affected by c and t_s. With increasing t_s and c, birefringence after transient shearing grows faster and achieves higher values. When the long chain concentration increases to $c/c^* = 0.5$, we observe a qualitative change in the evolution of birefringence during transient shearing. The loci of $I_\perp/I_{tot}$ for B0 and

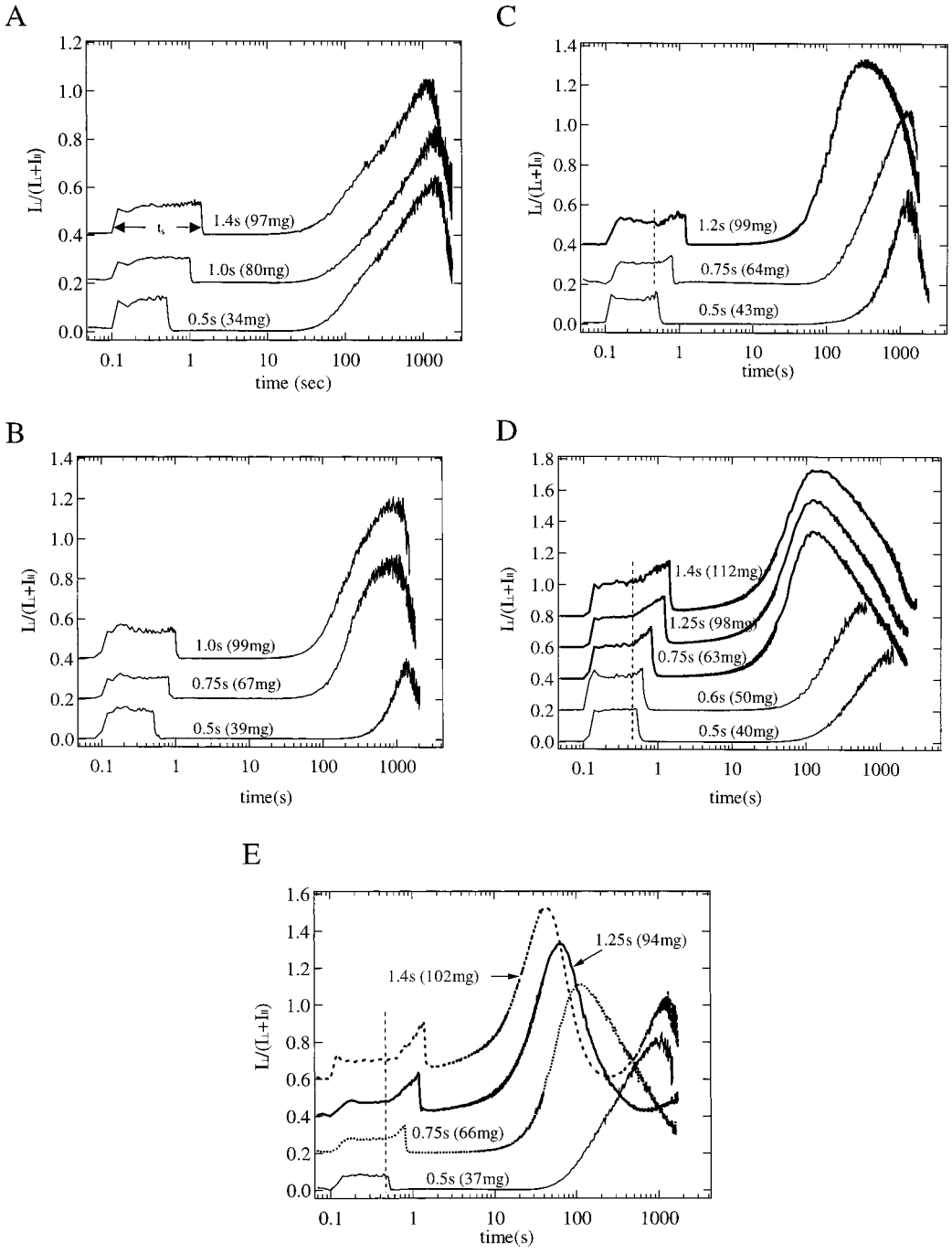

Figure 7. Relative intensity through crossed polarizers ($I_\perp/I_{tot}$) of (A) B0, (B) B025, (C) B05, (D) B1, and (E) B2 during and after short-term shearing at 0.14 MPa and 137 °C is plotted against time. Time is offset by 0.1 s and relative intensities have been shifted progressively by an offset of 0.2 for clarity. Shearing time and w_{ex} are given above each trace. Dotted lines in figures indicate the time when the birefringence upturn during shear can be observed.

B025 during transient shearing at 0.14 MPa generate the same boxlike shape as that sheared at lower σ_w; however, for B05, B1, and B2, we see that $I_\perp/I_{tot}$ exhibits an "upturn" during shear after the plateau value is reached and then relaxes upon cessation of shear (Figure 7). The "upturn" feature, previously reported by Kumaraswamy et al. in a conventional Z−N iPP, was shown to correspond to the formation of a "shear-induced structure" that appeared as fiberlike crystalline reflections of the α-modification of iPP during real time synchrotron WAXD.[35,37] Subsequently, these samples were shown to have developed a skin-core crystalline morphology. In our samples, the "upturn" in birefringence similarly indicates that shearing at $\sigma_w > \sigma^*$ results in the formation of highly oriented structure in B05, B1 and B2. The "upturn" appears at $t_s = 0.35$ s in these three blends, corresponding to w_{ex} of approximately 65 mg. Moreover, it should be noted that the birefringence of B1 and B2 after transient shearing at $\sigma_w > \sigma^*$ does not completely relax to the baseline value when $t_s > 1$ s (Figure 6, parts D and E).

The ultimate value of birefringence (at the time the transmittance fell to zero) does not increase linearly with c but distinctively increases around $c/c^* = 0.5$. This nonlinear dependence on long chain concentration suggests that the kinetic and morphological consequences of increased long chain content are due to a multibody effect. Specifically, long chain−long chain overlap en-

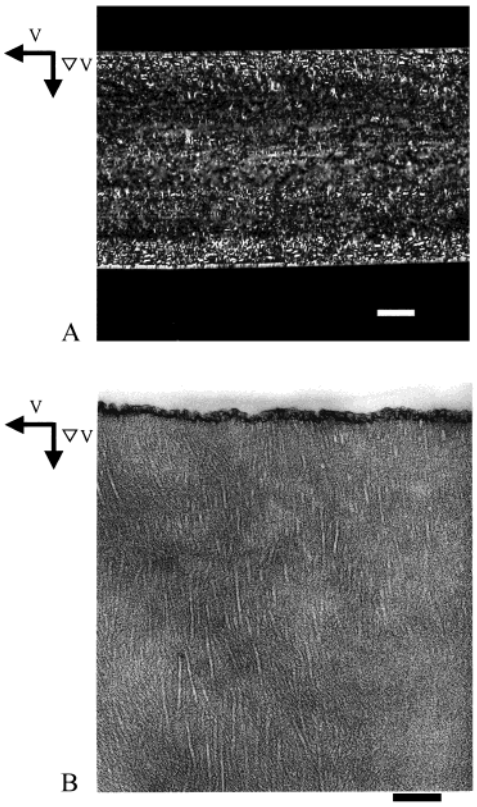

Figure 8. (A) Optical and (B) transmitted electron micrographs of B2 crystallized at 137 °C after shearing at $\sigma_w = 0.07$ MPa for $t_s = 7.5$ s, corresponding to $w_{ex} = 98$ mg. Scale bar is (A) 100 μm and (B) 100 nm.

hances the development of anisotropy during shearing, i.e., the appearance of the birefringence "upturn", and leads to well-developed oriented structures during subsequent crystallization.

3.3.3. Ex Situ Observation by OM and TEM. Optical micrographs (OM) under crossed polarizers and TEM for a B2 sample sheared at 0.07 MPa for 7.5 s ($w_{ex} = 98$ mg) and then crystallized at $T_c = 137$ °C for 2800 s are presented to show the typical morphology of blends sheared at $\sigma_w < \sigma^*$ (Figure 8). The value of $I_\perp/I_{tot}$ just before removing the sample was 0.075 ± 0.03. A thin (5μm thick), somewhat oriented skin layer can be seen at the surfaces of the sample, and a fine-grained layer of spherulitic structures is observed below the skin layer. The thin birefringent skin layer is composed of stacked lamellae grown perpendicular to the flow direction (Figure 8B).

All blends crystallized after shearing at σ_w of 0.14 MPa > σ^* showed a highly oriented skin layer (Figure 9, parts A−E). The skin layers appear as bright bands at the walls when viewed through crossed polarizers. The thickness of the skin layers for B0, B025, B05, B1, and B2 (Figure 9, parts A−E) are estimated to be 10 ± 3, 25 ± 10, 53 ± 5, 47 ± 8, and 47 ± 5 μm, respectively. The thickness and uniformity of the skin layer increases remarkably at c/c^* of 0.5 and saturates for $c/c^* = 1$ or higher. The abrupt transition between the skin layer and the spherulitic core provides a measure of the threshold stress required to induce the transition to oriented growth, σ^*, since the stress decreases linearly from the wall to the center of the flow channel. At depths greater than 50 μm from the wall, highly oriented crystallites are not observed; the boundary is fairly sharp and corresponds to $\sigma^* \approx 0.12$ MPa. The saturation in skin thickness as a function of long chain content indicates that the threshold stress varies weakly with c for $0.5c^* < c < 2c^*$ (Figure 5). As previously reported,[35] the formation of the oriented skin observed ex situ correlates with the development of strong birefringence in situ after cessation of shear as lamellae grow transverse to the precursors created during shear (Figures 7 and 9).

TEM images of the skin layer of the same samples examined by OM reveal shish kebab structures (Figure 10). The thickness of the bright skin layer observed by OM is consistent with the distance from the surface to the boundary between the row-nucleated region and the spherulitic region seen in TEM images. From a series of TEM images (Figure 10A−E), it can be clearly seen that the number of shish kebabs increases with increasing c and increasing t_s (Figure 10, parts D and F). Thus, evidence strongly supports the notion that the strong, nonlinear effect of c on the transient birefringence during shear-induced crystallization at $\sigma_w > \sigma^*$ is caused by the appearance of the shish kebab structure and the nonlinear increase in the number of shish kebabs particularly as c/c^* increases from 0.25 to 0.5.

4. Discussion

4.1. Isolating the Effect of Long Chain Content. To clarify the effect of the long chains, it is necessary to compare experiments performed at the same wall shear stress so that the average polymer orientation in the melt during shear is approximately fixed. Using this approach, we avoid the difficulty of discriminating the effects of long chain content from the highly nonlinear effects of changing the applied stress, which obscure the interpretation of prior studies that made comparisons at fixed deformation rate.[7,14−15,17−18,20−21] The addition of a small concentration of narrow distribution long chains to a fixed "base resin" exposes their role in oriented crystallization. The utility of this method was demonstrated by Kumaraswamy et al. who showed that long chain content in bidisperse blends was strongly related to the induction of oriented growth by shearing.[22] At fixed stress, and hence roughly fixed average orientation, the long chains become more oriented than average. The relative length of the long and short chains largely determines the disparity in their relaxation times and their orientation states during shear. In contrast to earlier experimental studies in which polymer samples with very broad molecular weight distributions were blended to vary long chain content,[32] Kumaraswamy used relatively well-defined materials. Thus, it was possible to be specific about the relative length of the long chains compared to the bulk ($M_L/M_S \sim 4.5$).

In the prior study by Kumaraswamy et al., concentrations above long-chain overlap were examined (2−10%, corresponding to c/c^* of 2.5−12.3), and pronounced skin formation was observed for all binary blends investigated (but not for either the short or long polymers alone). The purpose of the present study is to learn more about the mechanism by which long chains affect flow-enhanced crystallization. Here, we examine the change in behavior as a function of c both above c^* and below c^* to determine whether the long chain effect is a single-chain effect or cooperative. We further examine the experimental results for evidence of the specific steps in flow-enhanced crystallization in which the longest chains play an important role.

4.2. Sequence of Events in Shear Enhanced Crystallization. According to the model of Janeschitz-

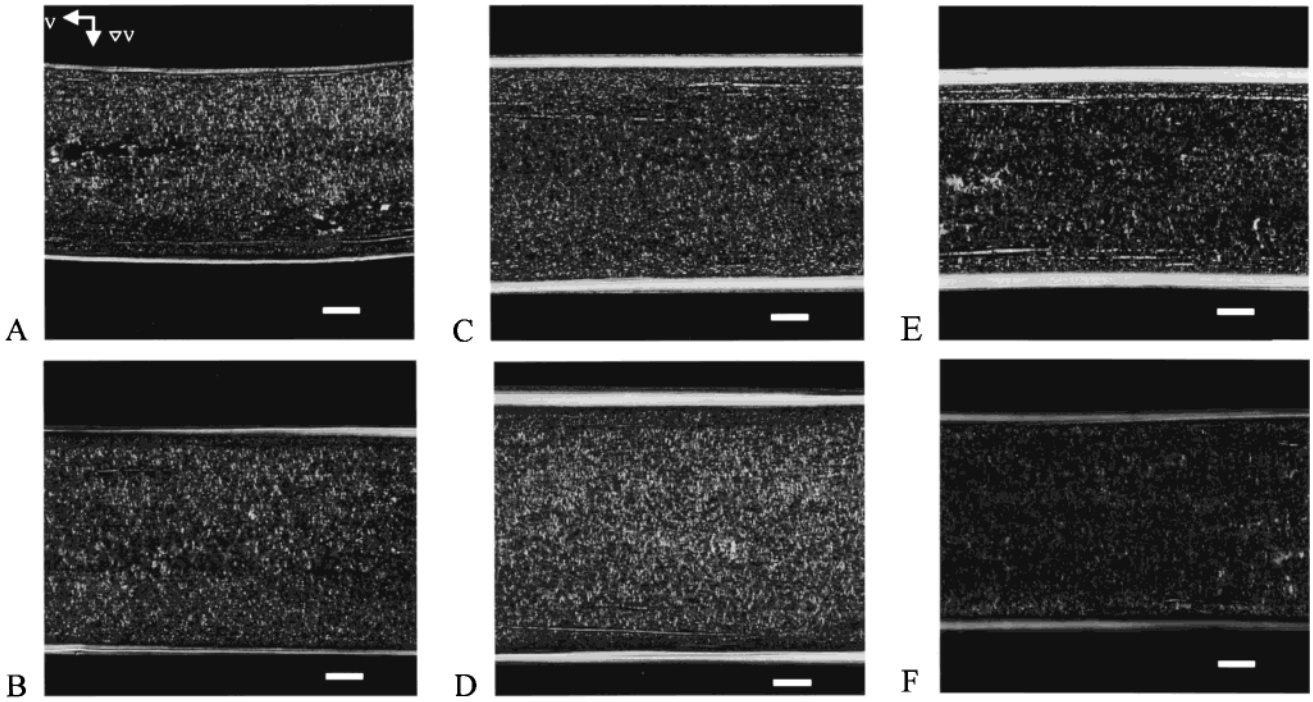

Figure 9. Optical micrographs viewed through polarizer and analyzer at ±45° with respect to the flow direction of (A) B0, (B) B025, (C) B05, (D) B1, (E) B2, and (F) B1 crystallized at $T_c = 137$ °C after shearing at $\sigma_w = 0.14$ MPa for $t_s =$ (A) 1.4, (B) 1.0, (C) 1.2, (D) 1.4, (E) 1.0, and (F) 0.6 s. Corresponding w_{ex} were 97, 99, 99, 112, 91, and 50 mg, respectively. The samples were quenched after crystallizing for (A) 1855, (B) 1611, (C) 1667, (D) 2899, (E) 1690, and (F) 550 s. The in situ birefringence and TEM images are presented in Figures 7 and 10. Scale bars are 100 μm.

Kriegl and co-workers,[7] the first stage in shear-enhanced crystallization is the formation of "pointlike" precursors; once formed, sustained shearing can elaborate these "pointlike" precursors into "threadlike" precursors (Figure 11). The high aspect ratio of the threads causes lamellar growth from them to be laterally constrained, resulting in formation of a highly oriented, row-nucleated morphology. Our data is qualitatively consistent with this model, and we will discuss our results in the context of this basic physical picture. From the earlier work of Kumaraswamy et al.[22] and the present results, it is clear that long chains play a central role in the formation of the row-nucleated morphology. Within the framework put forward by Janeschitz-Kriegl, it is essential to know where the long chains are involved in the sequence of events that underlie the creation of this oriented structure.

The observed behavior of the blends indicates that the long chains greatly enhance the growth of threadlike precursors, but only mildly enhance the formation of the initial pointlike precursors. Above the threshold stress, the elaboration of pointlike nuclei into threads depends strongly on c. TEM images reveal the number of threads increases with increasing long chain concentration (Figure 10), holding T, σ_w, t_s, and γ_w all nearly fixed. As concentration increases from 0 to 0.5c*, we observe an increase in thread length per unit volume up to a saturation value that does not change substantially with further increase in long chain concentration up to 2c* (corresponding to approximately 100 nm between thread centers). For B0 and B025, most threads are less than 20 μm long (both ends visible in TEM images), but for B05, B1, and B2, the length of the threads exceeds the field of view (20 μm).

Further evidence for increased thread length comes from the real-time development of birefringence during crystallization after cessation of shear. The birefringence grows faster for blends with higher long chain concentration up to $c = c$* and exhibits a saturation effect at higher concentration, consistent with the ex situ TEM findings (Figure 7). The increasing birefringence during crystallization is due to the growth of oriented lamellae (kebabs) that occurs after the cessation of flow. The quiescent growth velocity is the same for all blends as indicated by our DSC data and transient turbidity (Figure 1), so the accelerated growth of birefringence with increasing c is a result of higher thread length per unit volume. Therefore, we conclude that long chains enhance the process of thread elaboration, leading to longer threads and higher thread density.

The transient birefringence observed during shear also shows that adding long chains enhances the formation of oriented precursors up to concentrations of c*, with a weak effect upon further addition of long chains. For low concentrations of long chains (B0 and B025, Figure 7, parts C−E), the birefringence profile is box-like, tracking the orientation of chain segments in the melt due to the applied stress. When more long chains are added, there is an "upturn" in the birefringence (beginning at roughly 0.35 s for B05, B1 and B2, Figure 7, parts C and D), which prior work has shown correlates with the formation of threadlike precursors and highly oriented α-iPP with c-axis along the flow direction.[35,37] The "upturn" occurs when a sufficient number of oriented crystallites (combination of "shish" and "kebabs") have formed, causing the birefringence due to crystalline anisotropy to become greater than the birefringence from segmental anisotropy in the melt. Thus, the appearance of the "upturn" for $c/c^* \geq 0.5$ indicates a substantial increase in the number and length of threadlike nuclei with increasing long chain concentration.

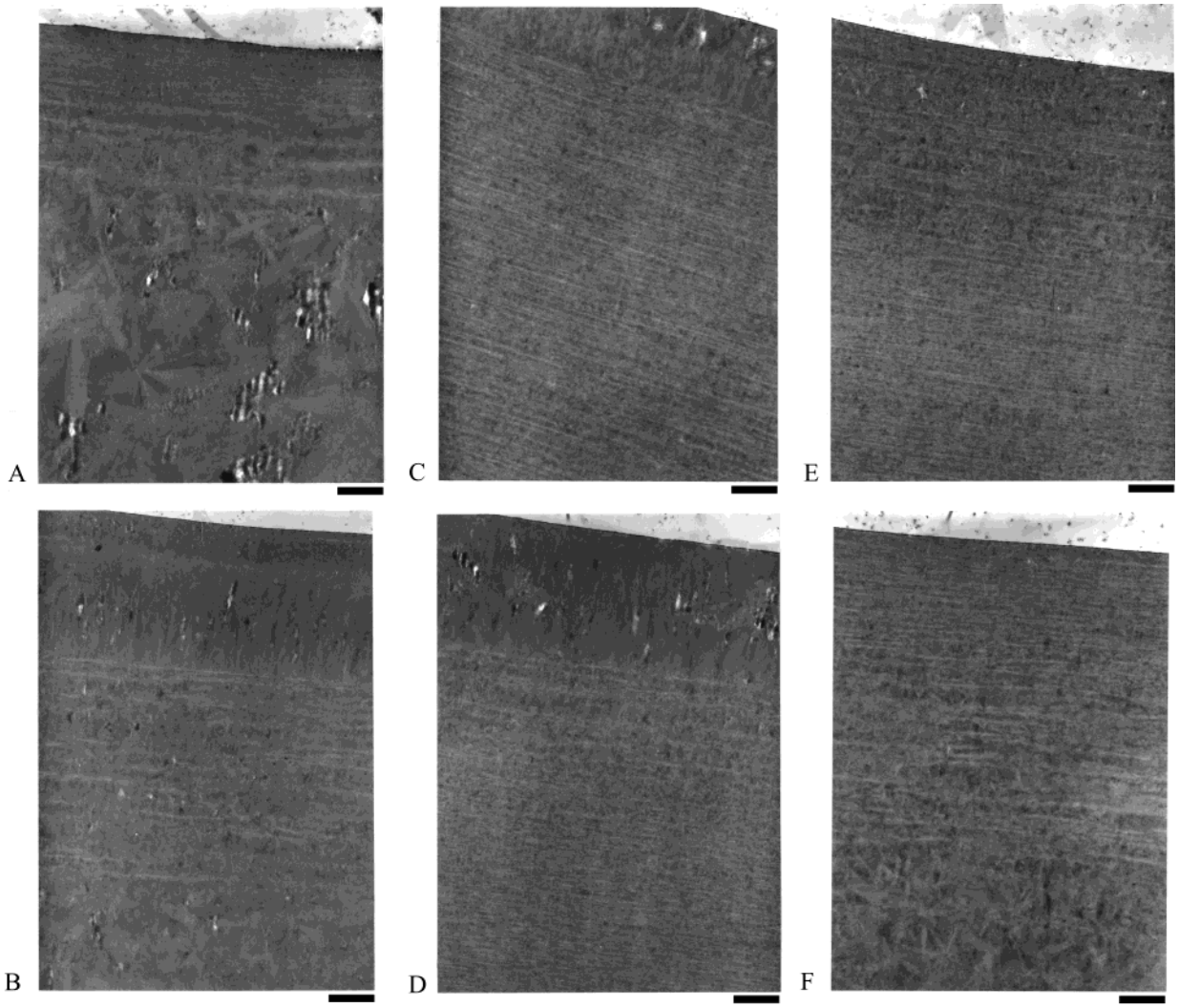

Figure 10. TEM micrographs of the skin layer of (A) B0, (B) B025, (C) B05, (D) B1, (E) B2, and (F) B1 for the same shearing and crystallization conditions as Figure 9. The flow direction is parallel to the edge of the sample shown as the boundary between the sample (gray) and the embedding material (white). Sections were cut in the plane of the flow and velocity gradient directions. Scale bars are 2 μm.

In contrast to the strong effect of c on the formation of threadlike precursors, the effect of long chains on the formation of the pointlike precursors was relatively weak. Below the critical stress required to induce highly oriented growth, the absence of oriented structures observed by ex situ microscopy implies that threadlike precursors were not formed or that they were exceedingly short-lived and did not nucleate oriented crystallization. Nevertheless, samples sheared below the threshold stress show accelerated crystallization kinetics compared to quiescent conditions. Indeed, the fine-grained layer seen in samples sheared below σ^* shows an increased number of spherulites when compared with quiescent conditions, consistent with the shear-induced formation of pointlike precursors. The density of nuclei in a sheared melt is a function of stress and temperature. In our isothermal experiment, the stress gradient determines nuclei density and spherulite size, with large spherulites forming at the core where few nuclei develop and a fine-grained layer near the wall (optical micrographs of samples subjected to $\sigma_w < \sigma^*$, not shown). TEM images for quenched samples sheared at $\sigma_w > \sigma^*$ reveal that, below the oriented skin layer, spherulites at a given depth from the wall (i.e., at comparable $\sigma < \sigma^*$) were approximately the same size regardless of c. Thus, the addition of long chains did not produce a pronounced change in morphology for $\sigma < \sigma^*$, suggesting that long chains do not strongly affect the formation of point nuclei. In situ rheo-optical observations also support this conclusion. The accelerated formation of pointlike precursors at $\sigma < \sigma^*$ is manifested in the development of light scattering at earlier time than in the quiescent case. The addition of long chains has only a weak effect on turbidity half times for experiments at similar stresses ($\sigma_w < \sigma^*$) and shearing times (Figure 12).

4.3. Comparison to Existing Concepts regarding the role of Long Chains. Somani et al.[14] have offered a molecular picture for nucleation and growth induced by transient shearing mediated by chains above a critical orientation molecular weight M^*. In their results, stacked lamellae oriented perpendicular to the flow direction were observed by TEM. Assuming the power law relationship between the shear rate and M^* ($M^* \sim \dot{\gamma}^{-a}$) given by Keller,[42-43] they estimated M^* from the fraction of the oriented crystalline lamellae. Implicit in this analysis is the assumption that "only polymer molecules having a molecular weight above a critical orientation molecular weight M^* can form oriented structures"[14] at a given shear rate and that all chains

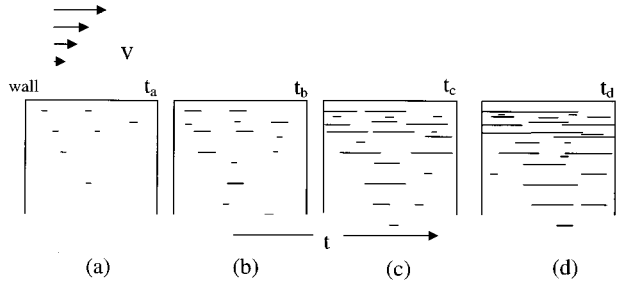

Figure 11. Schematic diagram of Janeschitz-Kriegl's model for the formation of the skin layer induced by applying shear above the threshold shear stress. (a) Point nuclei appear in the super cooled melt at t_a. The number density of the nuclei decreases with increasing depth from the wall. (b) Threadlike precursors grow in the flow direction from the point nuclei that appeared at t_a. The lateral growth of lamellae (not shown) from threadlike precursors begins. Additional pointlike precursors form during the period from t_a to t_b. (c) As threads become long enough that lateral growth would suppress noncrystallographic branching, the template for an oriented skin is created. (d) Further increase in the number and length of threads leads to greatly increased overall crystallization rate and highly oriented growth.

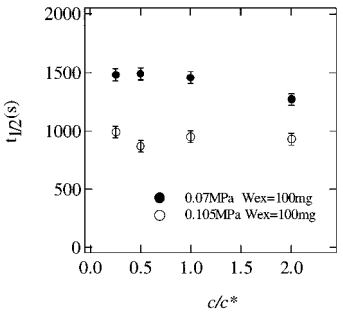

Figure 12. Turbidity half-time ($t_{1/2}$) to reach $I_{tot}/I_{tot}(0) = 0.5$ vs long chain concentration (c/c^*) for conditions where highly oriented growth did *not* occur ($\sigma_w = 0.07$ and 0.105 MPa, for maximum t_s).

above M^* are in these oriented crystals. In a subsequent paper,[32] they argue that incorporation of short molecules into the oriented crystals may not take place. The present results show that the amount of oriented crystalline material (approximately half of the polymer in the oriented skin) can greatly exceed the amount of long chains (less than 1.5% in the present blends) that are involved in templating the oriented growth. Physically, this result suggests that it is sufficient to create a very dilute quantity of threads to template oriented growth, which incorporates chains of all lengths as the growth front advances.[41]

Keller et al.[13,42−43] ascribed the mechanisms for formation of threadlike structures to a coil−stretch transition of long molecules from random coils to extended conformations which can then solidify into fibrillar crystals. His explanation of a coil−stretch mechanism at work during simple shear flow was based upon studies in extensional flow, where shish were interpreted to be the result of extended chain crystals. In shear flow, Keller hypothesized that extension of long chains would result between entanglement constraints imposed by the surrounding molecules. Our data suggest multibody interactions of long chains play a significant role during the formation of threads, exhibiting a nonlinear increase in the number of threads with increasing c. While we do not believe a coil−stretch transition occurs during shear, the nonlinear dependence on long chain concentration may indicate that long chain−long chain entanglement plays a role, consistent with the partial extension of segments of the long chains due to topological constraints described by Keller.

4.4. Molecular Perspective on Shear-Enhanced Crystallization. 4.4.1. Formation of Pointlike Precursors. Even at low stress levels, flow greatly enhances the crystallization kinetics of a polymer melt by increasing the number of point nuclei. The mechanism by which these crystallization precursors are formed is unknown, but the results indicate that the mechanism does *not* preferentially involve the most oriented chains in the melt (the long chains). Put another way, it appears that the average level of segmental orientation is the dominant factor in determining their rate of formation, since the rate appears to be governed by the local stress (∼average orientation), nearly independent of the concentration of long chains. Thus, the experimental results negate our initial hypothesis that the addition of long chains would greatly enhance the formation of pointlike nuclei following shear as a result of the stronger orientation of the longest molecules due to their long relaxation times. Similarly, Somani et al.[14] have hypothesized that for "orientation-induced crystallization, a certain degree of molecular extension must be achieved to induce formation of stable primary nuclei" and for a "particular $\dot{\gamma}$, only the longer chains will be oriented." If this were the case, the addition of long molecules would increase the amount of oriented material as well as the number of primary nuclei. Alternatively, Janeschitz-Kriegl and co-workers suggested that the pointlike precursors form by the coalescence of "athermal nuclei" during shear, tracking the applied strain rather than the degree of molecular orientation.[38] This mechanism is expected to be insensitive to the addition of long chains, in accord with these results. However, the "athermal nuclei" hypothesis does not agree with the observed temperature dependence of precursor formation.[22,35]

The α-modification of crystalline iPP is a complex arrangement of molecules composed of 3_1 helices with alternating handedness packed into a monoclinic unit cell.[39] Although shear cannot generate this precise structure, the local ordering of segments due to flow increases the likelihood that chains may adopt a long-lived structural arrangement due to thermal motion. The accelerated formation of pointlike precursors occurs sporadically at a rate that is controlled by the average segmental orientation. The fact that the presence of highly oriented long chains does not greatly affect this rate implies that many chains are involved, sampling a significant portion of the overall orientation distribution.

4.4.2. Formation of Threadlike Precursors. The primary mechanism by which long chains enhance the formation of row-nucleated structures appears to be the elaboration of pointlike precursors into threads. When the applied shear stress exceeds the critical shear stress, threadlike precursors form. The fact that the threshold stress σ^* initially decreases with addition of long chains (Figure 5) shows that the presence of these slower relaxing molecules enhances the elaboration of pointlike precursors into threads.

Why are long chains preferentially involved in elaboration into threads? If we consider the propagation of a threadlike precursor from a pointlike precursor, we envision that adjacent chains in the melt interact with

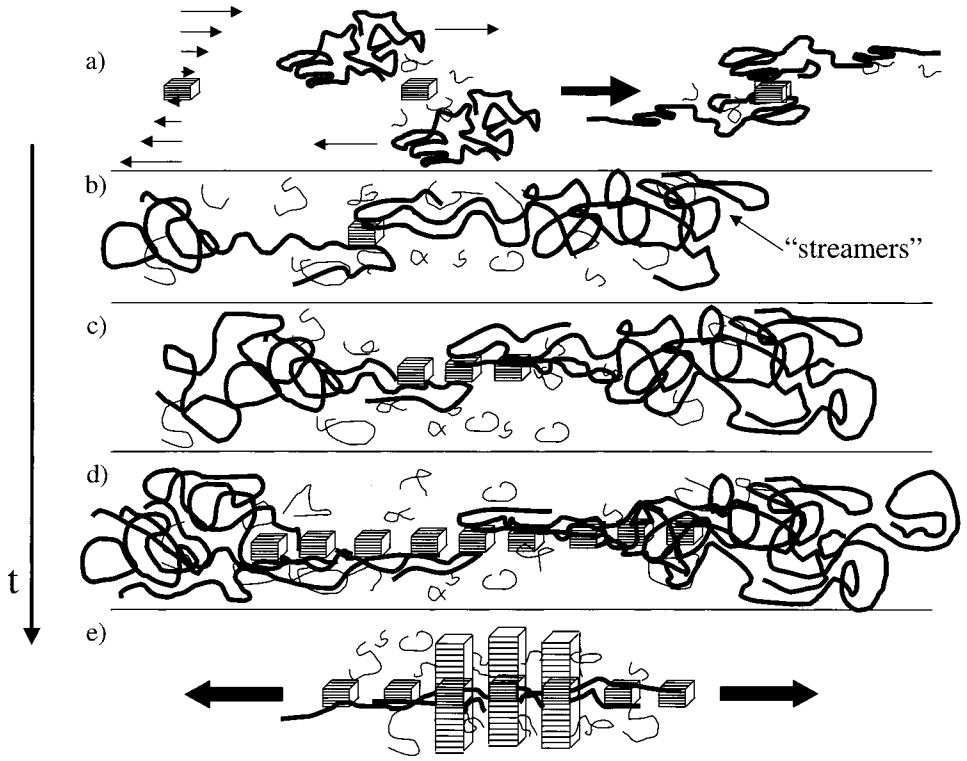

Figure 13. Schematic diagram of the nature of shear induced nucleation and subsequent growth of oriented crystalline lamellae during short-term shearing above the threshold shear stress. (a) A long chain (bold line) dispersed in short chains in a supercooled polymer melt adsorbs to an existing pointlike precursor as it flows past. Dangling segments of adsorbed chains become oriented due to sustained shear. (b) Additional chains adsorb and their dangling segments form "streamers" upstream and downstream of the pointlike precursor. (c) The increased local orientation of the chain segments increases the probability that long-lived ordered structures will form. (d) More chains adsorb to these new nucleation sites and the process propagates a string of nuclei along the line of flow. (e) The nuclei along this thread lead to lateral lamellar growth.

the surfaces of a given pointlike precursor. Suppose that an adjacent chain adsorbs to a surface normal to the gradient direction: the free segments of such a chain will subsequently become elongated due to sustained shear (Figure 13a). Chain segments convected along a streamline with lower velocity relative to the attachment point will lag behind, while those segments on the higher velocity side will be extended downstream. If a number of chains become tethered to the pointlike precursor, this process will create a substantial number of oriented segments upstream and downstream of the particle (Figure 13b). Although full extension is unlikely, the strong orientation enhances the likelihood of subsequent nucleating structures forming along the line of flow (Figure 13c). Thus, the same process can repeat itself over and over again, leading to a train of precursor clusters, connected into a thread (Figure 13d).

Long chains might greatly enhance this process for three reasons. First, their segments are more oriented than average, which might put them in a preferred state for adsorption onto a precursor surface. Second, simply by virtue of having more segments per molecule, they are more likely to adsorb. Third, once adsorbed, they provide more segments to participate in "streamers" dangling upstream or downstream (Figure 13b), and these segments will be more oriented on average than those of shorter "streamers."

After cessation of shearing, lateral growth continues from the threadlike precursors. Since relaxation of chains in the melt occurs quickly after cessation of shearing, the growth velocity is expected to be that of the quiescent case.

Why is the threshold stress insensitive to long chain concentration? We expected σ^* to decrease substantially with increasing long chain concentration over the range tested, due to stronger relative orientation and proximity of long chain segments. Instead, we see a threshold stress that only decreases ~10% as c increases to $0.5c^*$ and is almost unchanged with further increase to $2c^*$ (Figure 5). The schematic picture in Figure 13 may provide insight into the reason(s) that addition of long chains enhances the formation of threads, yet the threshold stress does not change with long chain concentration. It appears that a threshold orientation determined by the relative molecular weights of the chains (M_L/M_S) and the applied stress, is required to induce the propagation of threadlike precursors. This threshold is insensitive to c over the range probed, because the relaxation time of the long chains does not increase greatly from that of isolated long chains in a short chain matrix (even at $2c^*$ there is little long−long entanglement).

Why is the effect of long chains cooperative? There are two ways in which long chain−long chain overlap might be significant. First, the probability of a particularly strong local enhancement of orientation due to overlap of the "orientation clouds" represented by individual long chains becomes increasingly likely to occur. In view of our speculation about the way the threads propagate, the multibody interaction may be among long chain "streamers" trailing from pointlike precursors. Second, the relaxation time of the long chains increases with increasing long chain−long chain interaction, particularly with the inception of long chain−long chain

entanglement. As the long chain relaxation time increases with c, the orientation of the long chains also increases, particularly for c low enough that the mean relaxation time is hardly perturbed (so the deformation rate under a given stress remains nearly that of the pure short chains). Similarly, if a long chain adsorbs to the surface of a precursor, the degree of orientation of the resulting "streamers" will be higher if the strands are entangled with surrounding long chains that are being swept by in the flow.

Why do shish not tumble? A striking feature of the row-nucleated morphology is that the threadlike precursors are well-oriented along the flow direction. If they tumbled with the vorticity of the shear flow, it is unlikely that they could attain the lengths seen in micrographs or exhibit the strong, uniform orientation that is observed. It may be that the threads do not tumble because they are elongating continuously. For long, slender particles, the tumbling period, which is deduced from Jeffery orbit for rodlike particles,[40] increases strongly with increasing length of rods. We suspect that the threadlike precursors may grow sufficiently quickly that their tumbling period effectively becomes infinite (long compared to t_s) before they tumble. The shish formed in B025 after shearing at 0.14 MPa for 1.0 s were not completely straight (Figure 14A), whereas the shish formed in B2 after shearing at 0.14 MPa for 0.75 s were quite straight and thin (Figure 14B), perhaps reflecting the difference in thread growth velocity in these samples.

Why does the concentration of threads saturate? It is interesting that the addition of long chains beyond c^* to $2c^*$ produces little further enhancement of the formation of threads. This may be related to a morphological feature observed ex situ. The distance between centers of neighboring shish in the region where shish are most densely packed was determined from TEM images. For the same conditions (σ_w = 0.14 MPa; comparable strain units, corresponding to $w_{ex} \sim$100 mg) the shortest distance between shish for B0 was 200 nm and for all other blends 100 nm. Since TEM images average over the thickness of the ultrathin sections, the actual spacing between the threads may be greater than this apparent value. Nevertheless, the distance between threads seems to saturate as c increases. We see two general mechanisms that might be involved in this saturation effect. First, once the threads reach a sufficiently high density, they may hinder each other's further growth (perhaps growing threads strike lateral lamellae propagating from neighbors). Second, at the tip of a growing thread, locally like a pointlike precursor, there may only be sufficient surface area for adsorption of a small number of chains. As the concentration of long chains increases, they may fully occupy the available surface, causing the propagation velocity of the threads to saturate.

5. Conclusions

Blending well-characterized iPP into a "base iPP" is a useful way to determine the relationship between characteristics of specific molecules and their role in the crystallization process.[22] Using this approach we have shown that addition of less than 1% of chains with M_w five times larger than the M_w of the base resin profoundly affects the crystallization kinetics and crystalline morphology from a sheared melt. Beyond unambiguously demonstrating the important role of long chains in the formation of anisotropic crystallization under flow, this approach allows us to be specific about the length that is meant by "long chains" and the concentration of these chains in the melt.

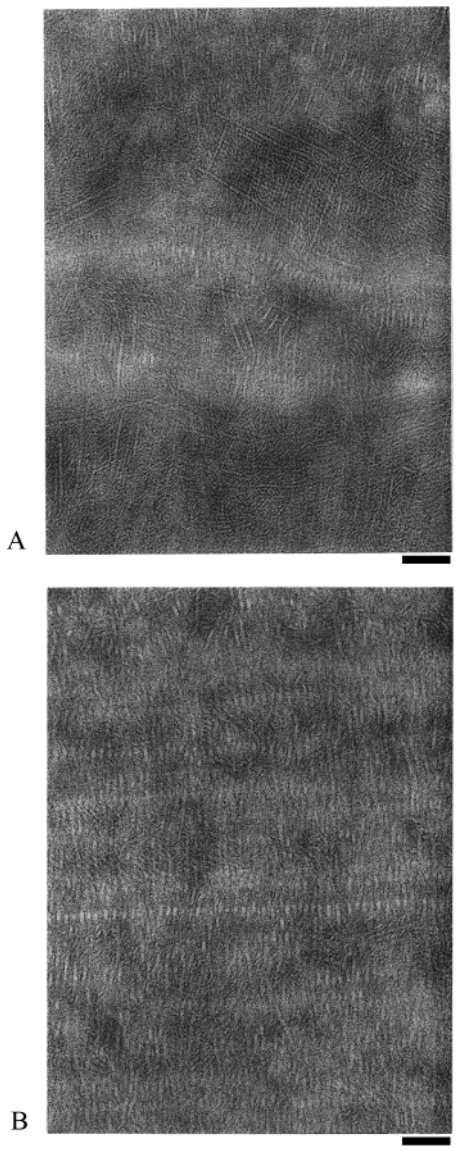

Figure 14. TEM micrographs of the skin layer of (A) B025 and (B) B2 crystallized at T_c = 137 °C after shearing at σ_w = 0.14 MPa for similar total strain ($w_{ex} \sim$100 mg), corresponding to t_s = (A) 1.0 and (B) 0.75 s. Scale bars are 100 nm.

Varying the concentration from below to above c^* revealed that the effect of the long chains involves cooperative interactions, evident in the nonlinear relationship of the long chain concentration, particularly as c approaches the long chain−long chain overlap concentration.

The long chains greatly enhance the formation of threadlike precursors, but only mildly enhance the formation of pointlike precursors.

To clarify how long chains promote the transition to oriented growth, future work should include the following: (1) quantifying the orientation of the long chains, (2) determining the relationship between their relative length (M_L/M_S) and the threshold stress σ^*, and (3) measuring the local thread length per unit volume as a function of the local stress ($\sigma-\sigma^*$). Such results would give us greater insight into the molecular factors that determine the propagation velocity of threads, which is

central to understanding the crystallization kinetics and morphology induced by flow.

Acknowledgment. Financial support was provided by the National Science Foundation (DMR-9901403).

References and Notes

(1) Flory, P. J. *J. Chem. Phys.* **1974**, *15*, 397.
(2) Kobayashi, K.; Nagasawa, T. *J. Macromol. Sci. (Phys.)* **1970**, *B4*, 331.
(3) Bushman, A. C.; McHugh A. J. *J. Appl. Polym. Sci.* **1997**, *64*, 2165.
(4) Ziabicki, A. *Colloid Polym. Sci.* **1974**, *252*, 207.
(5) Okamoto, M.; Kubo, H.; Kotaka, T. *Macromolecules* **1998**, *31*, 4223.
(6) Ulcer, Y.; Cakmak, M.; Miao, J.; Hsiung, C. *J. Appl. Polym. Sci.* **1996**, *60*, 669.
(7) Liedauer, S.; Eder, G.; Janeschitz-Krigel, H. *Int. Polym. Process.* **1995**, *3*, 243.
(8) Hill, M. J.; Keller, A. *J. Macromol. Sci. (Phys.)* **1969**, *B3*, 153.
(9) Hill, M. J.; Keller, A. *J. Macromol. Sci. (Phys.)* **1971**, *B5*, 591.
(10) Pennings, A. J.; Keil, A. M. *Kolloid Z. Z. Polym.* **1965**, *205*, 160.
(11) Garber, C. A.; Clark, E. S. *J. Macromol. Sci. (Phys.)* **1970**, *B4*, 499.
(12) Fritzsche, A. K.; Price, F. P. *Polym. Eng. Sci.* **1974**, *14*, 401.
(13) Keller, A.; Kolnaar, H. W. H. Flow Induced Orientation and Structure Formation. In *Processing of Polymers*; Meijer, H. E. H., Ed.; VCH: New York, 1997; Vol. 18.
(14) Somani, R. H.; Hsiao, S.; Nogales, A.; Srinivas, S.; Tsou, A. H.; Sics, I.; Balta-Calleja, F. J.; Ezquerra, T. A. *Macromolecules* **2000**, *33*, 9385.
(15) Jerschow, P.; Janeschitz-Kriegl, H. *Int. Polym. Process.* **1997**, *12*, 72.
(16) Sherwood, C.; Price, F.; Stein, R. *J. Polym. Sci. (Polym Symp.)* **1978**, *63*, 77.
(17) Lagasse, R. R.; Maxwell, B. *Polym. Eng. Sci.* **1976**, *16*, 189.
(18) Vleeshouwers, S.; Meijer, H. *Rheol. Acta* **1996**, *35*, 391.
(19) Duplay, C.; Monasse, B.; Haudin, J. M.; Costa, J. L. *J. Mater. Sci.* **2000**, *35*, 6093.
(20) Andersen, P. G.; Carr, S. H. *Polym. Eng. Sci.* **1978**, *18*, 215.
(21) Wolkowicz, M. D. *J. Polym. Sci.: Polym. Symp.* **1978**, *63*, 365.
(22) Kumaraswamy, G.; Kornfield, J. A.; Yeh, F.; Hsiao, B. S. *Macromolecules* **2002**, *35*, 1762.
(23) Janeschitz-Kriegl, H. *Rheol. Fundam. Polym. Proc.* **1995**, 409.
(24) Janeschitz-Kriegl, H.; Eder, G. *J. Macromol. Sci.—Chem.* **1990**, *A27*, 1733.
(25) Eder, G.; Janeschitz-Kriegl, H.; Liedauer, S. *Prog. Polym. Sci.* **1990**, *15*, 629.
(26) Eder, G.; Janeschitz-Kriegl, H. *Mater. Sci. Technol.* **1997**, *18*, 268.
(27) Kusano, Y.; Morioka, T. *Polym. Prepr., Jpn.* **1996**, *45*, 3278.
(28) Seki, M.; Nakano, H.; Yamauchi, S.; Suzuki, J.; Mastushita, Y. *Macromolecules* **1999**, *32*, 3227.
(29) de Gennes, P. G. *Scaling Concepts in Polymer Physics*; Cornell University Press: Ithaca, NY, 1979.
(30) Takahashi, Y.; Isono, Y.; Noda, I.; Nagasawa, M. *Macromolecules* **1985**, *18*, 1002.
(31) Ballard, D. G. H.; Cheshier, P.; Longman, G. W.; Schelten, J. *Polymer* **1978**, *19*, 379.
(32) Nogales, A.; Hsiao, B. S.; Somani, R. H.; Srinivas, S.; Tsou, A. H.; Balta-Calleja, F. J.; Ezquerra, T. A. *Polymer* **2001**, *42*, 5247.
(33) Kumaraswamy, G.; Verma, R. K.; Kornfield, J. A. *Rev. Sci. Instrum.* **1999**, *70*, 2097.
(34) The effect of holding time after filling polymer melt in the flow cell on crystallization kinetics was checked. The crystallization kinetics measured by birefringence and turbidity for samples after holding for more than 5 min at 215 °C were identical within the error.
(35) Kumaraswamy, G.; Issaian, A. M.; Kornfield, J. A. *Macromolecules* **1999**, *32*, 7537.
(36) Sano, H.; Usami, T.; Nakagawa, H. *Polymer* **1986**, *27*, 1497.
(37) Kumaraswamy, G.; Verma, R. K.; Issaian, A. M.; Wang, P.; Kornfield, J. A.; Yeh, F.; Hsiao, B. S.; Olley, R. H. *Polymer* **2001**, *41*, 8931.
(38) Janeschitz-Kriegl, H.; Ratajski, E.; Wippel, H. *Colloid Polym. Sci.* **1999**, *277*, 217.
(39) Lotz, B.; Wittmann, J. C. *J. Polym. Sci.* **1986**, *24*, 1541.
(40) Jamieson, A. M.; Gu, D.; Chen, F. L.; Smith, S. *Prog. Polym. Sci.* **1996**, *21*, 981.
(41) Dean, D. M.; Rebenfeld, L.; Register, R. A.; Hsiao, B. S. *J. Mater. Sci.* **1998**, *33*, 4797.
(42) Pope, D. P.; Keller, A. *Colloid Polym. Sci.* **1978**, *256*, 751.
(43) Keller, A.; Kolnaar, H. W. H. *Mater. Sci. Technol.* **1997**, *18*, 189.

MA011359Q